

We are IntechOpen, the world's leading publisher of Open Access books Built by scientists, for scientists

6,900

Open access books available

186,000

International authors and editors

200M

Downloads

Our authors are among the

154

Countries delivered to

TOP 1%

most cited scientists

12.2%

Contributors from top 500 universities



WEB OF SCIENCE™

Selection of our books indexed in the Book Citation Index
in Web of Science™ Core Collection (BKCI)

Interested in publishing with us?
Contact book.department@intechopen.com

Numbers displayed above are based on latest data collected.
For more information visit www.intechopen.com



Nanocrystalline Porous Silicon: Structural, Optical, Electrical and Photovoltaic Properties

Ma. Concepción Arenas¹, Marina Vega², Omar Martínez³
and Oscar H. Salinas⁴

¹*Departamento de Ingeniería Molecular de Materiales, Centro de Física Aplicada y Tecnología Avanzada, Universidad Nacional Autónoma de México, Santiago de Querétaro, Querétaro*

²*Centro de Geociencias, Universidad Nacional Autónoma de México, Querétaro*

³*Universidad Politécnica de Guanajuato, Av. Universidad Norte S/N, Juan Alonso Cortazar, Guanajuato*

⁴*Universidad Tecnológica Emiliano Zapata del Estado de Morelos, Morelos, México*

1. Introduction

In the electronics industry, crystalline silicon is the most widely used semiconductor. A great variety of electronic devices can be built based on silicon, from discrete to low and very high scale integrated circuits. One of the most common commercial applications is the photovoltaics; in fact, silicon is found in 90% of solar cells for terrestrial applications. Silicon has an indirect band gap of 1.12 eV and emits light weakly near the infrared region by phonon assistance. This fact limits its use in optoelectronic applications, where semiconductors such as GaAs and InP dominate this field. However, the photoluminescent and electroluminescent properties of porous silicon (Bisi et al., 2000; Canham, 1990) have generated great interest in optoelectronic devices. Porous silicon was accidentally discovered by Uhlir at Bell laboratories in the middle of the 1950 s. He found that, under the appropriate conditions of applied current and solution composition, silicon did not dissolve uniformly but instead fine pores (holes) were produced. Porous silicon (PS) is a semiconductor in nanocrystalline form (NPS), which could improve some properties of silicon, given that some properties, such as the electricals, are determined by the short range order of atoms, rather than by the long range order. In recent years, the great interest in NPS has been due to the high surface area of porous silicon, which has been useful as a model of crystalline silicon surfaces in spectroscopic studies (Anderson et al., 1990; Bisi et al., 2000; Dillon et al., 1992; Gupta et al., 1991), as a precursor to generate thick oxide layers on silicon and as a dielectric layer in capacitance chemical sensors. In addition, NPS has been applied in optoelectronics, micro-optics, energy conversion, environmental monitoring, wafer technology, micromachining and biotechnology. In the photovoltaic field, the application of NPS has not been widely explored. The first NPS cell with a crystalline silicon substrate was reported in 1992 by Smestad (Smestad et al., 1992). Nevertheless, until now, its main application in solar cells has been as a non-reflecting layer (Vitanov et al., 1997). The use of semiconducting polymers to form hybrid heterojunctions with NPS represents another potential application of porous silicon; it has been found

that the conductor polymer increases the effective conductivity of NPS as a function of the polymer penetration into the silicon pores (Jung et al., 1995; Moreno et al., 1999). This kind of heterojunction can improve the stability of light emitting devices (LEDs) and has formed structures with interesting photoluminescence (Nguyen et al., 2003; Parkhutik et al., 1994) and electroluminescence properties (Bsiesy et al., 1995). In this chapter, several topics are discussed, ranging from the study of NPS structure formation from monocrystalline silicon by electrochemical etching in acid electrolyte solution to the construction and evaluation of optoelectronic devices based on these structures, including the formation and electrical evaluation of hybrid heterojunctions based on nanocrystalline silicon structures and semiconducting polymers.

2. General aspects of nanocrystalline porous silicon

Nanocrystalline porous silicon (NPS) is composed of silicon wires and pores, and thus, it is a material with a large surface area (Bisi et al., 2000). It is obtained by the electrochemical dissolution of silicon (Si) wafers in aqueous hydrofluoric acid (HF) solution or by electroless etching in an HF solution containing an oxidizing agent (Arenas et al., 2006; 2008; Smith & Collins, 1992). The anodic dissolution in HF solutions is the main process used for this effect, where darkness or illumination is necessary for p-type or n-type silicon substrates, respectively, to achieve the etching process. In this section, a short description of NPS preparation and its structural and morphological characterization is presented.

2.1 NPS formation process

One of the most important advantages of porous silicon is its simple and easy preparation (Yu & Wie, 1992). Since the first studies in the middle of the 1950 s, NPS has been mainly obtained by the electrochemical dissolution of silicon wafers based on HF solution. This process consists of applying an anodic current to the silicon wafer in an HF electrolyte contained in a Teflon cell, which is composed of a silicon working electrode and a Pt counter electrode. The dissolution of silicon requires holes supplied from its valence band at its surface; thus, for n-type silicon, light is necessary to photogenerate holes in contrast to p-type silicon. A constant current density can adjust the porosity, thickness, uniformity and reproducibility of samples (Eddowes, 1990; Galun, 1995; Smith & Collins, 1992). Ethanol is added to the HF electrolyte to counteract the hydrophobic character of silicon and facilitate the infiltration of HF inside the pores. In addition, ethanol helps to remove the hydrogen bubbles generated during pore formation on the silicon surface. In the past, many studies of porous silicon formation have been limited exclusively to an electrochemical characterization of its current-voltage (I-V), relationships with the Schottky diode model of the semiconductor/electrolyte interface playing a predominant role. Although additional analysis techniques have been used recently to study porous silicon, its formation still arises from the I-V relationships, and a basic knowledge of silicon electrochemistry is essential to understand this process (Bard, 1986; Conway et al., 1983; Holmes, 1962; Vijn, 1973). Several reaction mechanisms for pore formation have been proposed (Bomchil, 1983; Eddowes, 1990; Lehmann & Föll, 1990; Smith & Collins, 1992; Turner, 1958). However, the most widely accepted was proposed by Lehmann and Gösele, as shown in Fig. 1. This mechanism is based on the oxidation of bonds on the silicon surface with the capture of holes and electron injection in four steps (Lehmann & Gösele, 1991):

1. A hole reaches the surface for a nucleophilic attack on Si-H bonds by fluoride ions from the HF electrolyte (i.e., the hole can then migrate on to a Si-H bond), thus releasing a proton.

2. A second attack is accomplished by another fluoride ion, causing the evolution of molecular hydrogen and electron injection into the substrate. The attack of the Si radical by fluoride causes electron injection into the silicon conduction band and the formation of a Si-F bond.
3. The next few steps involve the sequential removal of $-SiF_2$ by the replacement of protons in the highly oxidized silicon with the concurrent injection of an electron into the conduction band. A chemical reaction occurs in which HF is added across the one remaining Si-Si bond to release SiF_4 into solution, and in this step, a tetrafluoride (SiF_4) molecule is produced.
4. The tetrafluoride molecule reacts with two HF molecules and H_2SiF_6 is the final product in solution.

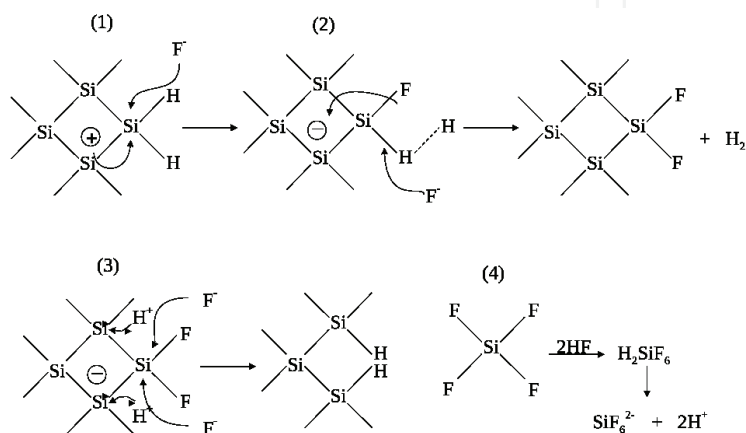
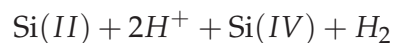
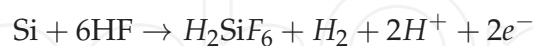


Fig. 1. Schematic of dissolution mechanism of silicon proposed by Lehmann and Gosele (Lehmann & Gösele, 1991).

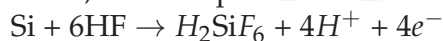
The dissolution mechanism is complex (Eddowes, 1990). In this reaction, only two holes are required to remove each silicon atom while one molecule of hydrogen is formed. Hydrogen is assumed to result from the reaction of protons or HF with an intermediate of the silicon oxidation reaction:



During pore formation, the following anodic semireactions occur:



However, an electropolishing process can also exist if the current density reaches the critical value, and this process can be described with the reaction:



The final properties, such as porosity and thickness of the nanocrystalline porous silicon layer, are very sensitive to many experimental variables, such as the doping density of the silicon substrate, the current density and the etching time, among others (Lehmann & Gösele, 1991; Searson et al., 1992). The porosity is an important parameter that determines the optoelectronic properties of NPS. Thus, it is necessary to determine porosity.

The porosity (P) is defined as the fraction of voids (air) within the nanocrystalline porous layer. This parameter could be estimated by gravimetry as described in Fig. 2, which shows the porosity produced by removed or dissolved silicon mass (m_r) during the etching divided by the total mass of etched silicon (m_T). In the porosity equation, m_1 is the silicon mass before etching, m_2 is the mass of the silicon substrate after etching (including porous silicon) and

m_3 is the substrate mass after dissolving the nanocrystalline porous silicon with a KOH (3 M) solution. In the same way, the film thickness of the nanocrystalline porous silicon layer can be estimated by considering the silicon density ($\rho=2328 \text{ mg/cm}^3$) and etched surface (S), $S=1 \text{ cm}^2$ as shown in Fig. 2.

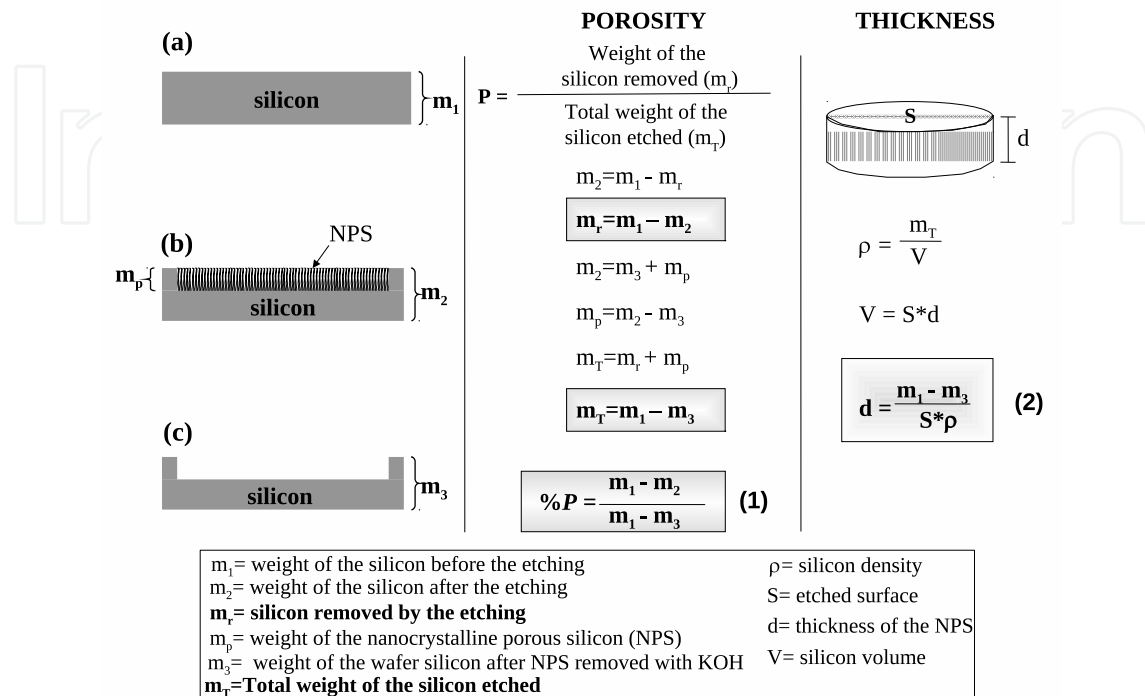


Fig. 2. Schematic representation of the method to calculate the porosity and thickness of nanocrystalline porous silicon by gravimetry (Bisi et al., 2000).

The porosity depends on the electrochemical etching conditions, such as the HF concentration and the type and resistivity of the silicon substrate. It has been observed that porous silicon porosity increases with current density at a given HF concentration. However, at a given current density, porosity decreases with HF concentration because HF is hydrophobic with silicon, which increases the difficulty of penetration/infiltration in the pores at high HF concentrations (Bisi et al., 2000). Fig. 3 shows the influence of the silicon substrate on the porosity and thickness of NPS layers. The porosity of the NPS layer obtained from a p-type substrate increases directly with the applied density current. In addition, it changes according to the silicon resistivity. More porous NPS layers are obtained from a silicon substrate of 10 Ω -cm of electric resistivity, whereas less porous NPS layers are obtained from lower resistivity silicon (0.002 Ω -cm). Starting from n-type silicon, the porosity increases as a function of current density, but these NPS layers are less porous than those obtained from p-type silicon. However, the film thickness (Fig. 3b) shows a linear behavior as a function of the current density, where values of greater thickness can be obtained with n-type silicon compared to p-type. In other words, with 10 Ω -cm n-type substrates, thick NPS layer with low porosity can be obtained, which, is related to an accelerated electrochemical etching. The discussion in the following sections correspond to NPS films from p-Si and n-Si obtained at the same conditions (20 mA, 1:1 ethanol: HF), unless otherwise noted.

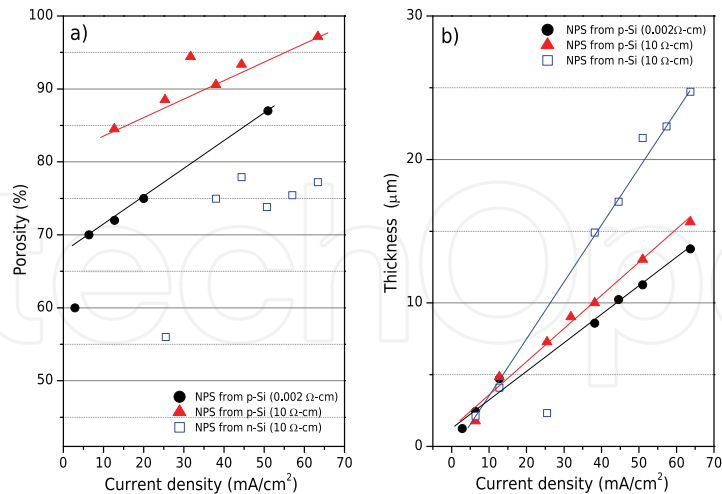


Fig. 3. Experimental a) porosity and b) thickness vs. current density of NPS films determined by the gravimetric method.

2.2 Structural characterization

2.2.1 Grazing-Incidence X-ray Diffraction

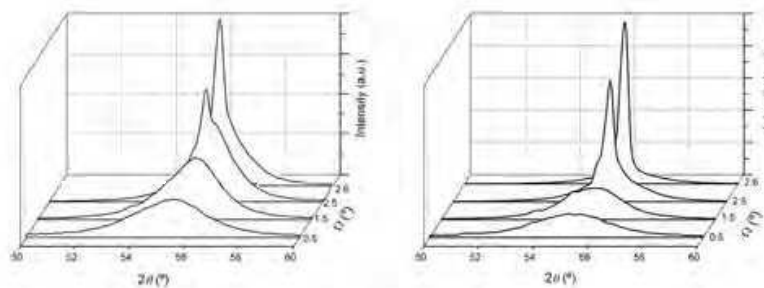


Fig. 4. Grazing-Incidence X-ray Diffraction of the nanocrystalline porous silicon from a) p-Si and b) from n-Si of approximately 10 µm (Arenas et al., 2008).

With Grazing-Incidence X-ray Diffraction (GID), it is possible to show that, as a result of the electrochemical treatment of crystalline silicon, a nanocrystalline thin film is obtained, as shown in Fig. 4. At small incidence beam angles, $\Omega < 2.5^\circ$ a broad reflection corresponding to the film is observed, whereas, at $\Omega = 2.6^\circ$ only the crystalline silicon diffraction peak is shown as an acute signal. Both kinds of signals are detected at $\Omega = 2.5^\circ$. A broad reflection indicates that its average crystal size is smaller than that of in the crystalline silicon according to the Scherrer equation (Patterson, 1939):

$$L = \frac{0.9\lambda}{B\cos\theta} \quad (1)$$

where λ is the wavelength of the incident X-rays (0.15406 nm), B is the half value breadth of the diffracted beam and θ is the Bragg angle. Thus, it was possible to estimate an average crystal

size, L , for the films. The results indicate that the average crystal sizes are in the nanometer range: $L=3.5$ nm for the film obtained from p-Si and $L=3.1$ nm from n-Si.

2.2.2 Surface molecular structure

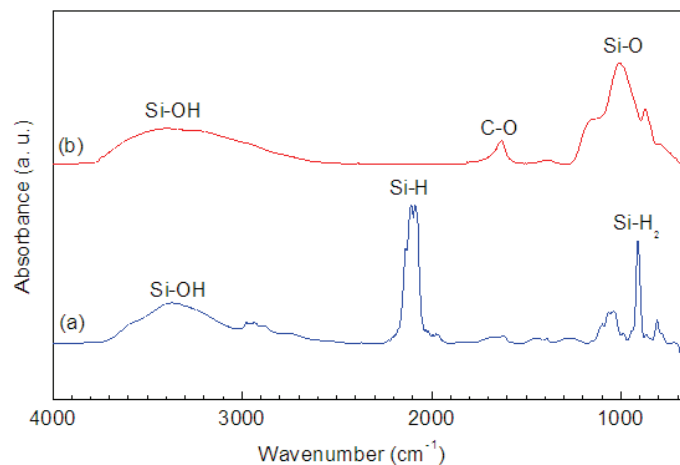


Fig. 5. Infrared spectra of NPS a) as prepared and b) oxidized at 300 °C.

The nanocrystalline silicon surface is saturated by hydrides (H^-) due to the nature of the electrochemical etching. The functional groups $Si - H_x$ ($x=1, 2, 3$) present in NPS can be identified by IR, as shown in Fig 5. The characteristic bands correspond to the molecular vibration of the bonds $Si - H_2$ at 910 cm^{-1} and Si-H at 2087 cm^{-1} (Beckmann, 1965; Bisi et al., 2000). It is possible to break these bonds easily by heating, light or exposure to gases and liquids, even after long periods of time under storage. Chemical stabilization of the surface is reached by controlled thermal oxidation; at 300 °C (Fig. 5b), the Si-H band disappears and a new band at 1000 cm^{-1} assigned to the Si-O bond vibration is observed (Fauchet et al., 1997). Other bands due to surface reactivity with the environment are summarized in Table 1.

2.2.3 Morphology by SEM and AFM

Nanocrystalline silicon film is a highly porous structure. It is composed of wires formed perpendicular to the surface, as can be observed using scanning electronic microscopy (SEM), as shown in Fig. 6a. Their length and diameter depend on the formation conditions and, therefore on the crystalline silicon type. From p-Si, wires with a diameter estimated by atomic force microscopy (AFM) between 130 and 160 nm are obtained, as shown in Fig. 6b, whereas, from n-Si, wire diameters are about three times smaller, between 30 and 60 nm, as shown in Fig. 6c.

3. Optical properties of NPS

Optical properties such energy band gap (E_g) and refractive index (n) of the NPS depend on the etching conditions, current density, electrolyte composition and type of silicon substrate (p-Si or n-Si). At high porosities, a blue shift of the optical absorption of NPS can be observed (Sagnes et al., 1993), i.e., the E_g and n can be modified.

Functional group	Wavenumber (cm^{-1})	Assignment
OH	3610, 3452	Si – OH y H ₂ O stretching
CH	2958, 2927, 2856	CH ₃ , CH ₂ y CH stretching
SiHF ₃	2314, 2245, 2206	—
SiH	2248, 2197, 2136, 2116, 2087, 2089, 2115, 2070	O ₃ – SiH, SiO ₂ – SiH, Si ₂ Si – SiH, Si ₂ H – SiH, and Si ₃ – SiH stretching
SiH ₂	2110	Stretching
CO	1630, 1720	—
CH ₃	1463	Asymmetric stretching
SiCH ₃	1230	Bending
SiO	1050, 1056-1160	O – Si – O stretching
Si – O – Si	1070	Asymmetric stretching
SiH	979/948	Si ₂ – H – SiH bending
SiH ₂	880-906, 908, 910	Scissoring
SiH ₂	856, 845	Wagging
SiO	827-832	O – Si – O bending
SiH	661	Wagging
SiH	624-650	Si ₃ – SiH bending
Si – Si	616, 620	Stretching

Table 1. Vibrational frequencies of NPS species by IR spectroscopy (Bisi et al., 2000).

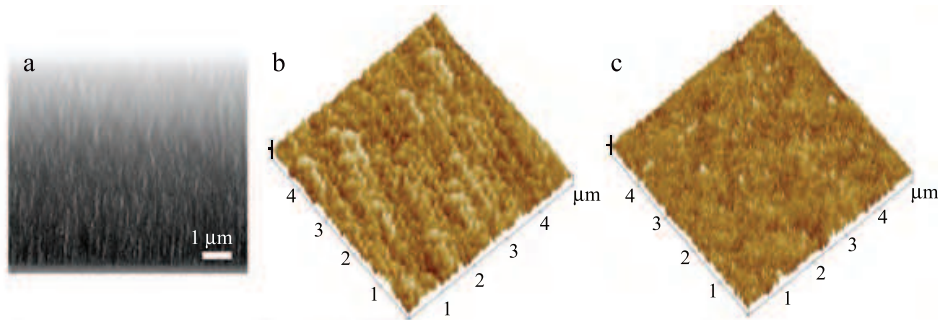


Fig. 6. Morphology of the nanocrystalline porous silicon film: a) SEM image of the transversal section from n-Si; b) 3D AFM image from n-Si, and c) 3D AFM image from n-Si. Scale in z= 30 nm/div.

3.1 Energy band gap of free standing NPS

The relationship of the optical transmittance (T) and absorption coefficient (α) of a semiconductor with thickness d is (Schroder, 1998):

$$T = \frac{(1 - R)^2 e^{-\alpha d}}{1 - R^2 e^{-2\alpha d}}. \quad (2)$$

If the reflectance of the semiconductor is almost null, $R \approx 0$ and equation 2 is simplified:

$$T = e^{-\alpha d}, \quad \alpha = -\frac{1}{d} \ln T. \quad (3)$$

The absorption coefficient is related to the semiconductor optical band gap (E_g) (Sze, 1990):

$$(\alpha h\nu)^\gamma = C(E_g - h\nu), \quad (4)$$

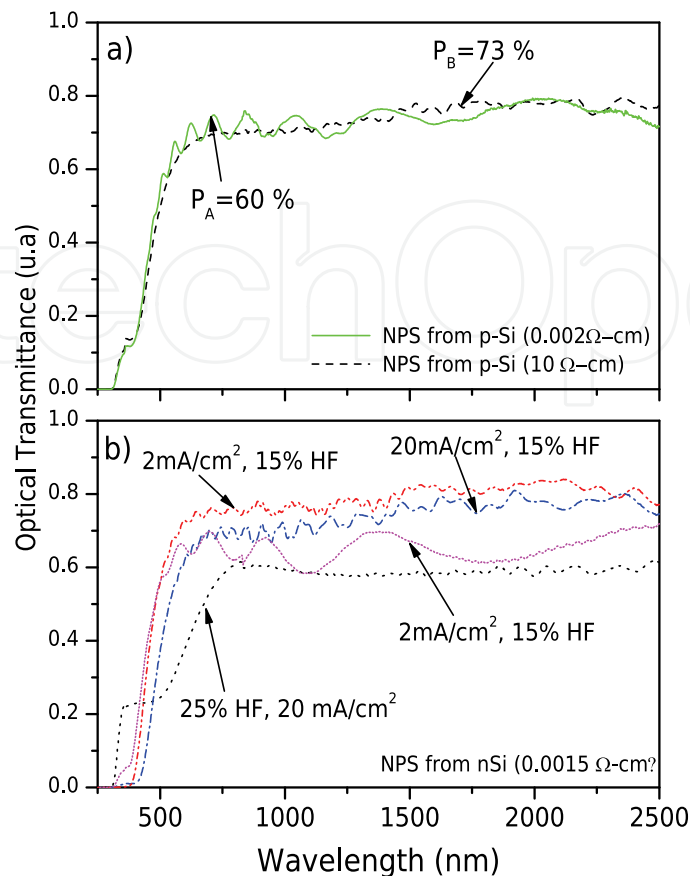


Fig. 7. Optical transmittance of free standing NPS films prepared using different anodization conditions.

where $h\nu$ is the photonic energy, C is a constant and γ takes values of 2 for direct transitions and 1/2 for indirect transitions.

The optical transmittance of free standing NPS films changes according to the porosity value and the anodization parameters, as shown in Fig. 7. Free NPS films with porosities of 60% and 70% show similar transmission spectra, but interference fringes that are well defined are only observed in less porous NPS films. The interference fringes are produced due to the light interference in the film. At low HF concentrations, the films show about 60% to 70% transmission, unlike the films prepared at high HF concentrations (Fig. 7b). The direct and indirect band gap of these free standing films are shown in Fig. 8 and Table 2. For direct transitions, the experimental E_g of the films is about 2.64 - 2.7 eV closer to the 3.3 eV value reported for powdered NPS supported between two transparent substrates by Feng (Feng & Tsu, 1994). The direct transition gives an E_g approximately 1.88 - 2 eV closer to those reported for NPS used in optoelectronic applications (Lugo et al., 1998; Peng et al., 1996; Sagnes et al., 1993). High concentrations (25%) of HF produce free standing NPS with larger E_g , which is distinctive of highly porous films, whereas, in low concentrations (15%), the less porous films show lower E_g values. Sagnes found that the E_g value can also be modified by the nanocrystalline size (Sagnes et al., 1993).

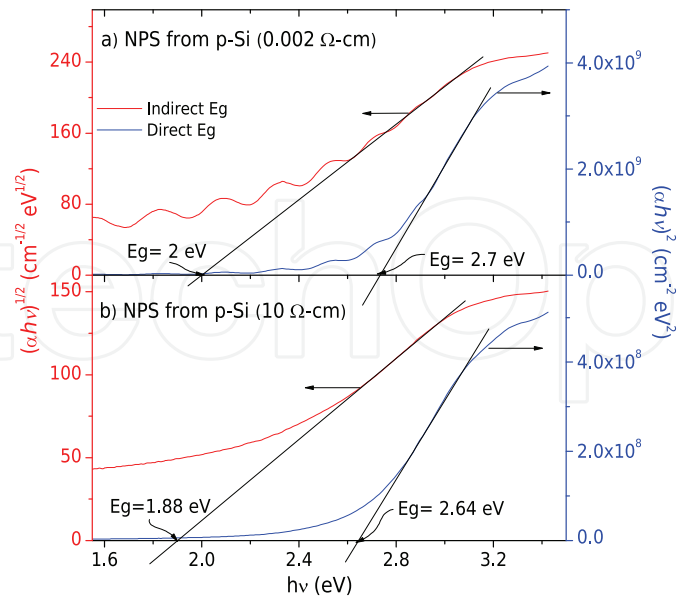


Fig. 8. a) Direct and b) indirect band gap of free standing NPS films obtained from p-Si.

NPS films from ($\rho = \Omega\text{-cm}$)	HF (%)	J (mA/cm ²), porosity, [Time, s]	Direct Eg (eV)	Indirect Eg (eV)
p-Si (0.002)	~14 %	2, 60%	2.7	2.0
p-Si (10)	25 %	20, 73%	2.64	1.88
n-Si (0.0015)	25 %	20	1.79	1.64
	15 %	20	2.85	2.64
	15 %	2, [1200]	2.96	2.9
	15 %	2, [480]	3.08	2.66

Table 2. Direct and indirect band gap of free standing NPS films prepared using different conditions.

3.2 Complex refractive index of NPS on silicon substrate

The optical reflectance of NPS on a silicon substrate is about 20 to 40% depending on the anodization conditions (Fig. 9). The main difference is in the amount of interference fringes, which are sensitive to the current density and thickness of NPS films (Arenas et al., 2010). This optical property determines important film parameters such as its refractive index and its extinction coefficient.

The NPS film is composed of air and silicon. Therefore, its refractive index (n) should range between 1.0 and 3.4. If the NPS is highly porous, n is closer to the refractive index of the air, and its value increases when the NPS films present low porosity (Arenas et al., 2010; Kordás et al., 2004). An algorithm is proposed to calculate the complex refractive index of NPS on crystalline silicon by means of reflectance spectra only (Arenas et al., 2010). Additionally, the NPS film thickness is determined by the normal reflectance spectra without information from its transmission spectrum (i.e., the separation of NPS films from the silicon substrate is not necessary). The algorithm is based on the analytical relations established by Heavens (Heavens, 1965) to obtain both the complex refractive index and thickness of an absorbing

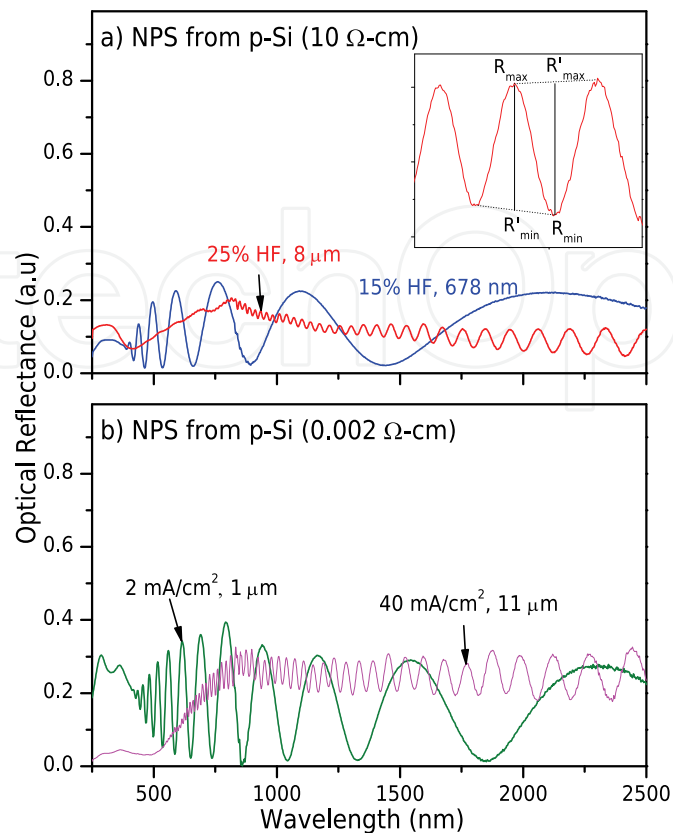


Fig. 9. Optical reflectance of NPS supported on a silicon substrate.

thin film on an absorbing substrate. Based on this model, some simplifications are introduced at different wavelengths. The model considers the maxima and minima of the interference fringes of reflectance spectrum (see inset Fig. 9a), and R_{max} and R_{min} are the assumed values for the continuous maxima (minima) envelopes using the following equation (Arenas et al., 2010):

$$\frac{1}{R_r} = \frac{4g_1g_2(1 - g_1^2 - g_2^2x^2 + g_1^2g_2^2x^2)x}{g_1^4 - 2g_1^2g_2^2x^2 + g_2^4x^4} \quad (5)$$

where R_r is defined as (Manificier et al., 1976; Swanepoel, 1983)

$$\frac{1}{R_r} = \frac{R_{max} - R_{min}}{R_{max}R_{min}} \quad (6)$$

The model is only valid in the range of 1000 to 2500 nm, where the absorption is almost constant. For the UV-Vis region, other considerations must be taken into account (Swanepoel, 1983; Torres et al., 2003). It was applied to NPS films obtained from p-Si substrates, as shown in Fig. 10. It was found that the refractive index of NPS films with 60, 70, 72 and 87% porosity is a function of this parameter, where n decreases at high porosities of NPS, which is consistent to the trend reported by Bisi (Bisi et al., 2000).

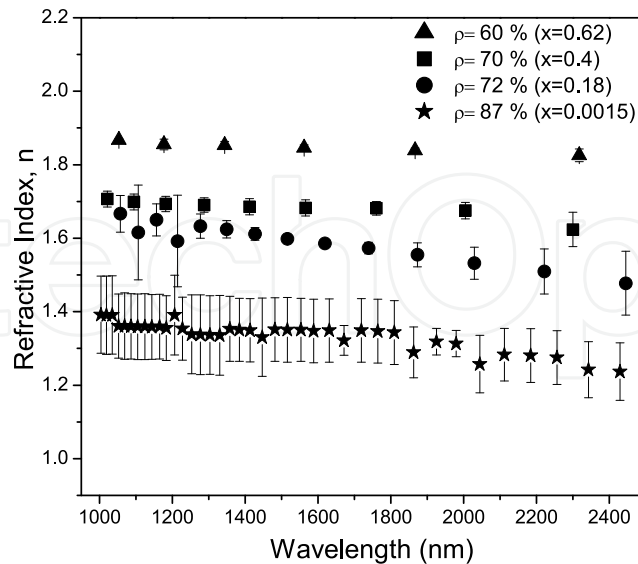


Fig. 10. Experimental refractive index of NPS supported on a silicon substrate (Arenas et al., 2010).

4. Electrical properties

4.1 Photoconductivity

The electrical current is the amount of electrons flowing in a unit of time. An electron is the elemental electrical charge in matter and its absence is called a hole. They are referred to as free charge carriers because they are free to move from one point to another inside matter. It is necessary to be aware that the particles that actually move in matter are electrons, and hole movement is only a consequence. This movement leads to electron flow; a continuous electron flow is one of the definitions of electrical current. When charge is flowing, there is an electrical current. Under most circumstance, charges in movement are confined within a limited region, in the interior of a metallic wire, the cylindrical volume of a neon tube, or the transversal section of an electron beam into a kinescope, for instance. Quantifying the current is the total charge crossing an area perpendicular to the flow per unit of time (s):

$$Q = \int_{t_1}^{t_2} I dt \quad (7)$$

Current originates from charge flow, and, inside of a conductor, these charges are electrons. Therefore, electron movement is the phenomenon responsible for electrical current. The coulomb is a magnitude that is defined by means of the elemental charge, which is the charge that the electron has, -1.602×10^{-19} C: 1 Coulomb = 6.242×10^{18} electrons

For an idea of the size of a coulomb, approximately 6242197253433208489 electrons are needed to form a charge of 1 C. Therefore, the amount of electrons passing a specific point at a given current level can be calculated. For example, if a current of eight amperes is crossing a cross sectional area over five seconds, approximately 2.497×10^{20} electrons flowed across the area.

Electrons movement inside matter has no velocity or acceleration constant due to interatomic interactions and the material characteristics at the atomic level. Thus, this movement is based on a phenomenon called diffusion or drift. The average velocity of electrons is approximately 4 m/h.

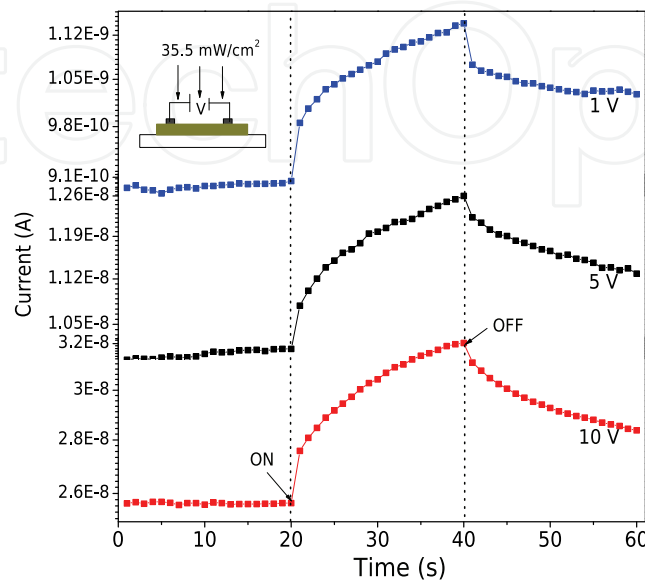


Fig. 11. Current as a function of time of the NPS film at three applied electrical voltages.

An electrical field, internal or external, is necessary to move electrons. Therefore, applying an electrical potential to the bulk or surface can create an electrical current. An electromotive source is used to apply a constant or variable external electrical field. It is a device that converts chemical, mechanical or solar energy into electrical energy, which is necessary to maintain a constant electrical charge flow. An electromotive source of one volt will perform one joule of work over every charge of one coulomb passing through it. Photoresponse characterization was performed for nanocrystalline porous silicon thin films to understand its sensitivity to light exposure, as shown in Fig. 11. The technique consisted of applying a fixed electrical potential on the material surface and recording the current under dark conditions after illumination for a determined period of time and continuing after another period of time without illumination. The current intensity of the NPS thin film is almost the same under dark and illuminated conditions, as shown in Fig. 11. Based on the plot of I vs. t , it is possible to estimate the total generated charge under an applied electrical potential under both dark and illuminated conditions using Eq. 7. The area under the curve is the result of the defined integral. The difference between the generated charge under light and under illumination is charge generated by light exposure, where

$$\text{generated charge} = \text{charge under light} + \text{charge under dark}. \quad (8)$$

When a material is highly conductive, there are fewer electrons due to illumination compared to electrons in the conduction band. If the material is almost intrinsic, the generation under light must be higher, but it also depends on the material band gap and the wavelength of light. The nanocrystalline porous silicon layer used in the characterization was almost intrinsic.

However, the charge generation was low, and thus, the material was not sensitive to this wavelength. The charge generated under illumination corresponded to $2.14450152 \times 10^{10}$ electrons (Fig. 11).

4.2 Metal - NPS junction

Metal - semiconductor (M - S) contacts are an essential part of the electrical performance of any semiconductor device because they are the communication channel between the world inside the device and the world outside of it, which is a simple way to describe the role of M - S contacts. The metal layer enables current to flow out of the device, allowing the external circuit to work with the purpose for which it was designed. M - S contacts are fabricated by depositing a metal layer over the semiconductor surface. Thus, both materials are in intimate contact (Table 3). Metal deposition can be done by vapor deposition (Carroll et al., 1966), metal sputtering (Murarka, 1983) and electroless techniques (Wolfgang, 1991), for example. Vapor is used in manufacturing to deposit thicker layers. If the device structure requires a thinner layer, the sputtering technique is used. Electroless techniques are also used for thinner layers. However, they are not used often in manufacturing due to cycle time and process issues. A technique is selected depending on the semiconductor device structure and application. Depositing a metal on the semiconductor implies forming an interface between two materials. The characteristics of this interface present many different issues, such as mechanical, physical, chemical, and mainly electrical issues. Why is necessary to deposit a metal layer over the semiconductor surface? The purpose is to protect to the semiconductor surface from the environmental conditions. Most semiconductors are easily oxidized; metals are less susceptible to oxidation. Therefore, the purpose of the metal layer is the protection of the semiconductor surface and mechanical support for the external terminal connections. Otherwise, the device performance would be unstable and easily degraded. Mechanical, electrochemical and physical issues at the interface impact the main behavior of interest: the electrical behavior.

Ohmic behavior	Rectifying behavior
Height barrier equals to zero (Rhoderick & Williams, 1998; Salinas et al., 2006; Sze, 1990)	Barrier height positive and not equal to zero.
Minimum resistance stated at the M - S interface.	Maximum or high resistance state.
Electrons and holes are able to flow to or from the semiconductor	Electrons can flow in only one direction.

Table 3. Electrical behavior of M - S contacts based on barrier height level.

Therefore, whether the current can flow to the external circuit depends on the electrical characteristics. The crystalline silicon industry is mature and manufactures electronic devices, and thus, the M - S interface issues have already been overcome or at least minimized. When a metal and a semiconductor are in intimate contact because the work functions of both materials are different, a built-in barrier is created at their interface (Salinas et al., 2006), which is called a Schottky barrier. The barrier height is directly related to the difference in the Fermi levels between the metal and semiconductor material. The larger the difference is, the higher will be the barrier height is. The barrier opposes the flow of the free charge carriers from one side to another. The electrical behavior of M - S contacts is identified depending on the barrier height (Salinas et al., 2006; Sze, 1990).

When a new semiconductor material is proposed to build electronic devices, research on the M - S interface must be done. For nanocrystalline porous silicon the panorama is not as clear as that for crystalline silicon. The electrical characterization of M - S with different metal layers must be done. If the Schottky barrier is equal or close to zero, an ohmic contact is expected. The current can flow inside or outside the device with minimum opposition, and the relationship between electrical potential (V) and current (I) is governed by *Ohm's* law (Salinas et al., 2006; Sze, 1990), the contact is considered ohmic. If the barrier height is not close to zero, a rectifying contact can be expected. An ohmic contact affects the electrical performance of the device with a minimum or insignificant impact. There is a condition of minimum resistance across the contact, and therefore, free charge carriers can flow in or out of the device. However, rectifying contacts play an important role in different applications. In addition to these two types of contacts, a third type of contact could be formed if the semiconductor is heavily doped. In this special case, the Schottky barrier is sufficiently thin to let carries tunnel across it instead of jumping to overcome the barrier. There are many considerations to keep in mind during the analysis of M-S behavior. One consideration, for example, is the interfacial states, which are present at the mechanical junction of the contact, such as unbonding atoms, a rough surface, and mechanical damage during the metal deposition. For an ideal M - S contact, interfacial states are not taken into account. If this assumption works, no deep analysis is needed. Otherwise, a different characterization technique must be used to find the electrical behavior of the interfacial states (Rhoderick & Williams, 1998). For ideal conditions, Schottky theory explains the interface behavior and establishes the method to estimate the barrier height value.

This theory is called Schottky in honor of the German physicist Walter H. Schottky, who developed it. According to Schottky theory:

If $\Phi_{metal} < \Phi_{p-semiconductor}$, a rectifying barrier must be formed at the interface.

If $\Phi_{metal} > \Phi_{p-semiconductor}$, an ohmic contact exists rather than rectifying behavior.

If $\Phi_{metal} > \Phi_{n-semiconductor}$, a rectifying barrier must be formed at the interface.

If $\Phi_{metal} < \Phi_{n-semiconductor}$, an ohmic contact exists rather than rectifying behavior.

Characteristics of the I vs. V curve of a Schottky junction can be described by the following equation (Rhoderick & Williams, 1998):

$$I = I_0 \left[\exp \left(\frac{qV}{nkT} \right) - 1 \right], \quad (9)$$

where I_0 is the reverse saturation current, which can be experimentally determined. If the transport mechanism for electrical current is given by thermoionic emission theory, the barrier height (ϕ_b) of the junction can be defined by the following equations:

$$I_0 = aA^{**}T^2 \exp \left(-\frac{q\phi_b}{kT} \right),$$

$$\phi_b = -\frac{kT}{q} \ln \left(\frac{I_0}{aA^{**}T^2} \right). \quad (10)$$

where A^{**} is the modified Richardson constant, which depends on the effective mass of electrons in the semiconductor (Rhoderick & Williams, 1998), T is the absolute temperature, a is the contact area, and k is the Boltzmann constant. In practice, this junction hardly meets the equation and can be described with the modified equation:

$$I = I_0 \exp\left(\frac{qV}{nkT}\right) \left[1 - \exp\left(-\frac{qV}{kT}\right)\right], \quad (11)$$

where the ideality factor of the diode, n , is almost independent of the electrical potential (V) and is greater than 1. The equation can be simplified as

$$I = I_0 \exp\left(\frac{qV}{nkT}\right) \quad \text{when } V > 3kT/q, \quad (12)$$

From this last equation, the parameters I_0 and n can be obtained from the intersection and slope of the straight line of the plot of $\ln I$ vs. V . However, it is recommended to obtain them from the plot of $\ln I/[1 - \exp(-\frac{qV}{kT})]$ vs. V of Eq. 11 because the straight line involves all values of V and not only the zone of V greater than $3kT/q$, which can determine the value I_0 with accuracy. The deviation of linearity due to other transport mechanisms is better seen when plotting $\ln I/[1 - \exp(-\frac{qV}{kT})]$ vs. V . Therefore, these recommendations are taken into account in this study to handle the experimental data of developed junctions.

Aluminum (Al), copper (Cu) and gold (Au) have work functions of $\Phi_{Al}=4.3$ eV (Brabec et al., 2001), $\Phi_{Cu}= 4.6-4.7$ eV (Rhoderick & Williams, 1998) and $\Phi_{Au}=5.1$ eV (Brabec et al., 2001), respectively. To generate contacts of crystalline silicon, p-Si (10 Ω -cm) with an acceptor density of $10^{15} \text{ cm}^{-3} = 10^{21} \text{ m}^{-3}$ and nSi(10 Ω -cm) with a donor concentration of $10^{14} \text{ cm}^{-3} = 10^{20} \text{ m}^{-3}$ were used.

According to the $I/[1 - \exp(-qV/kT)]$ vs. V curves of the metal contacts of p-type and n-type silicon with aluminum and copper (not shown here), the exponential behavior of the current in the potential range of -1 to 1 V is similar to a rectifier, and the rectifier ratio (F_R) at a given potential can be estimated with the following equation:

$$F_R = \frac{I_{max}}{I_{min}} \quad (13)$$

In the Cu:p-Si:Al contact, the rectifier behavior is governed by the Cu:p-Si contact because the Al:p-Si showed ohmic behavior:

- F_R is about 1.0×10^2 at ± 1 V.
- In the potential range of -1 V to 0.04 V, the reverse saturation current I_0 is 1.57×10^{-6} A and $n=1.04$
- Between 0.06 to 0.18 V, I_0 is 2.1×10^{-6} A and $n=2.4$
- The deviation of the ideal n value ($n=1$) could be due to the presence of the interfacial layer or recombination in the depletion region.
- Above 0.18 V a serial resistance 1239 ohms was determined by the procedure described in (Pierret & Neudeck, 1989).
- The high serial resistance could be due to the physical contact between copper and silicon.

The parameters of the Cu:n-Si:Al are the following:

- F_R is about 18 at ± 1 V.
- Under reverse bias, the linear behavior of the current indicates a decrement of the barrier height potential due to the interfacial layer.

- Between -1 to 0.05V, I_0 is 1.34×10^{-6} A and $n=1.09$. Therefore, the current is given by $I=1.34 \times 10^{-6} \exp(qV/(1.09kT))$.
- At 0.04 to 0.14 V, I_0 is 8×10^{-7} A and $n= 2.0$. The current is given by $I= 8 \times 10^{-7}$ A $\exp(qV/(2.0kT))$.
- The high value of n indicates that the current is limited by the recombination in the depletion zone, which can be described by;

$$I_r = I_{r0} \exp\left(\frac{qV}{2kT}\right) \left[1 - \exp\left(-\frac{qV}{kT}\right)\right], \quad (14)$$

where I_{r0} depends directly of the depletion weight.

- At high injection potential, the serial resistance is approximately 1799 ohms.

Fig. 12 displays the barrier height (ϕ_b) distribution of the silicon contacts with aluminum and gold metals. For the determination of the ϕ_b , it was assumed that the electrical current is governed by the thermoionic emission mechanism. Therefore, Eq. 10 was used. The Richardson constants (A^{**}) taken into account were $32 \text{ Acm}^{-2} \text{ K}^{-2}$ for p-Si and $112 \text{ Acm}^{-2} \text{ K}^{-2}$ for n-Si (Rhoderick & Williams, 1998).

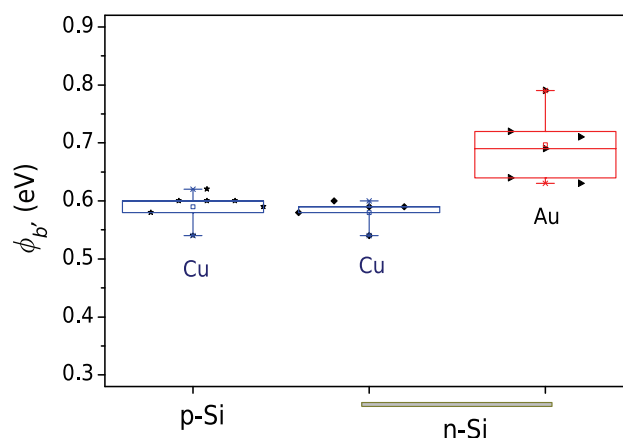


Fig. 12. Barrier height of metal contacts based on silicon.

5. NPS photovoltaic devices

5.1 Fundamental equations of a solar cell

A solar cell produces electrical energy by the absorption of solar irradiation without a secondary process. The electrical parameters of a photovoltaic device under dark conditions are given by (Sze, 1990)

$$I = I_0 \left[\exp\left(\frac{qV}{nkT}\right) - 1 \right], \quad (15)$$

where I is the current flow through the device under the influence of an electrical potential in direct bias V , I_0 is the reverse saturation current, n is the diode ideality factor, k is the

Boltzmann constant, q is the electron charge, and T is the temperature.

If $qV/nkT > 3$, the exponential term of the diode equation is predominant. Therefore, direct bias of the I vs. V curve is governed by

$$I = I_0 \exp\left(\frac{qV}{nkT}\right) \implies \ln I = \ln I_0 + \frac{qV}{nkT}. \quad (16)$$

where I_0 and n can be estimated with the extrapolation at $V = 0$ and the slope of the plot $\ln I$ vs. V , respectively.

Considering the resistances of the device, the equation diode is modified as

$$I = I_0 \left[\exp\left(\frac{q(V - IR_s)}{nkT}\right) - 1 \right] + \frac{q(V - IR_s)}{R_{shunt}}. \quad (17)$$

where R_s and R_{shunt} are the serial and shunt resistances.

Under illumination, the current is given by the following equation:

$$I = I_0 \left[\exp\left(\frac{q(V - IR_s)}{nkT}\right) - 1 \right] + \frac{q(V - IR_s)}{R_{shunt}} - I_L. \quad (18)$$

where I_L is the electrical current under illumination conditions.

The current under illumination for an arbitrary photovoltage is

$$I = I_0 \left[\exp\left(\frac{qV}{nkT}\right) - 1 \right] - I_L. \quad (19)$$

where I_{sc} is the short circuit current at $V = 0$.

If $I = 0$, Equation 19 is simplified to obtain (V_{oc}):

$$V_{OC} = \frac{kT}{q} \ln \left[\frac{I_L}{I_0} + 1 \right]. \quad (20)$$

The conversion efficiency, η , is given by

$$\eta = \frac{P_{max}}{A * P_{in}} * 100 = \frac{I_{sc} * V_{oc} * FF}{A * P_{in}} * 100, \quad (21)$$

where V_{oc} , is the open circuit voltage, I_{sc} the short circuit current, V_{max} , I_{max} and P_{max} are the voltage, current and power maxima, respectively, FF is the fill factor, A is the effective area (m^2) and P_{in} is the incident irradiation (W/m^2).

5.2 Photovoltaic NPS based devices

NPS is widely used in optoelectronic applications (e.g., photonic and electroluminescent devices). This nanocrystalline porous material has been used as a reflector layer in solar cell devices due its large light-trapping. Few works on the photovoltaic effect of NPS (Arenas et al., 2005; 2006;a; Smestad et al., 1992) indicate the need for continued research in this field to understand the mechanism charge carrier transport in NPS according to the type of silicon substrate, which is part for its fabrication.

NPS devices from p-Si and n-Si were fabricated using aluminum as the back contact and copper as the front contact. Both devices depicted the exponential behavior of the current under dark conditions, as shown in Fig. 13. The graphic adjusted to a diode rectifier with a

high confidence level. Experimentally, linear current behavior was found in the metal contacts of the Cu:NPS film and Al:p-Si substrate. Therefore, the rectifier behavior in the p-Si device is only attributed to the NPS:p-Si interface. In the NPS:n-Si device, the rectification contribution was mainly due to the Cu:NPS, shown in Table 4. The rectification ratio at ± 1 V was on the order of 10^3 for both devices. In fact, the NPS layer modified the electrical parameters of the silicon devices, J_0 decreased by four orders of magnitude and the resistance increased one order of magnitude. In all devices, the n values was far from that of an ideal diode, suggesting that the current transport was limited by the depletion zone (Pierret & Neudeck, 1989; Rhoderick & Williams, 1998).

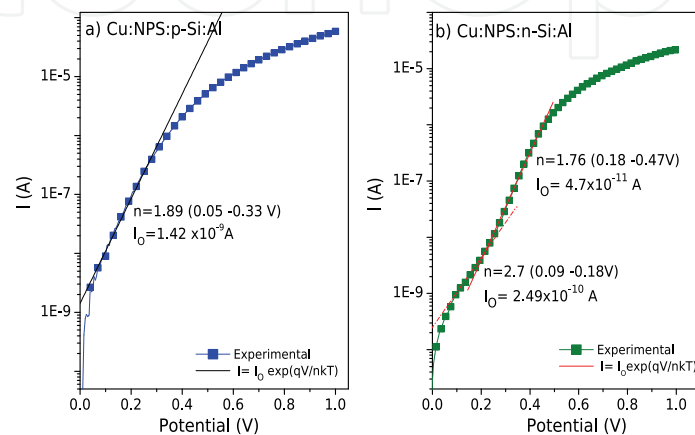


Fig. 13. Current - voltage curves under dark conditions of NPS devices based on p-Si and n-Si.

Under illumination, the photovoltaic effect is evident in the NPS devices, as shown in Fig. 14. The current density is about 0.13 to 0.32 mA/cm², and the open circuit voltage average is 235 mV for NPS:p-Si devices and 330 mV for NPS:n-Si devices. The photovoltaic effect was also observed in silicon devices without an NPS layer, suggesting that it is caused by the Schottky diode of the copper with the semiconductors. A thicker NPS film under the silicon substrate shows a similar behavior, indicating that the photovoltage is based on Cu:NPS and the Cu:n-Si junctions (Arenas et al., 2008).

Devices	J_0 (mA/cm ²)	F_R at $\pm 1V$	n (at V)	R_s (ohms)	J_{sc} (mA/cm ²)	V_{oc} (mV)	FF	η (%)
p-Si	0.17	1×10^2	2.03 (0.04-0.17)	1239	—	—	—	—
NPS:p-Si	1.59×10^{-4}	2×10^3	1.89 (0.05-0.33)	8557	0.13	235	0.33	0.016
n-Si	0.15	18	3.04 (0.07-0.29)	1799	0.32	355	Lower	—
NPS:n-Si	2.8×10^{-5}	1×10^3	2.7 (0.09-0.18)	18441	0.2	330	Lower	0.96

Table 4. Electrical parameters of NPS devices based on p-Si and n-Si.

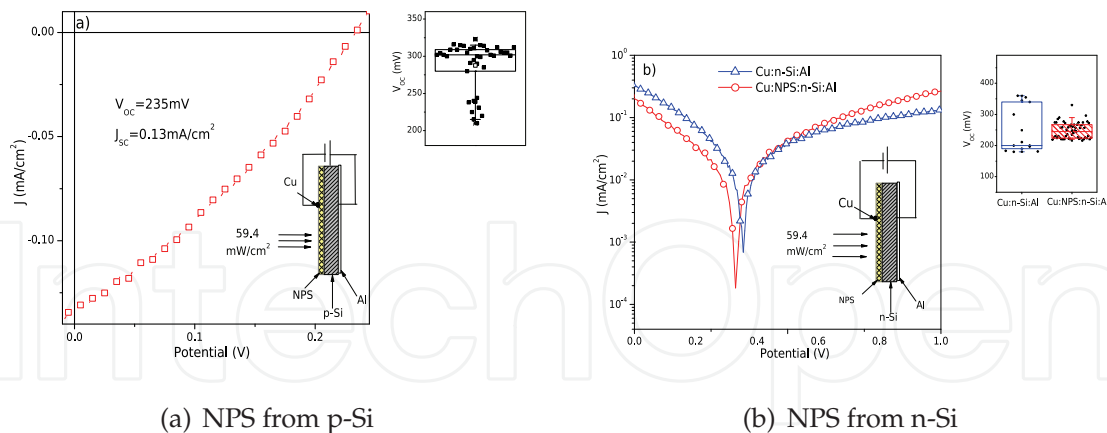


Fig. 14. J vs. V curves under illumination conditions of NPS devices from p-Si and n-Si (Arenas et al., 2008).

The contribution of the photocurrent and photovoltage in the heterojunction was monitored by the spectral response, as shown in Fig. 15. The relevant points for NPS:p-Si devices are described below:

- The photocurrent and photovoltage spectra are similar in the range of 1 to 3.5 eV of photon energy.
- Two zones are well defined, the first in the infrared region (1-1.47 eV) and the second in visible region (1.47 eV -3.25 eV).
- In the infrared region, the contributions are due to the absorption of bulk p-silicon, where the maximum peak consists of the energy band gap of bulk silicon.
- The contribution of NPS is evident in the visible zone, where the NPS presents high absorption (Eg 1.8 eV).
- Four smaller interferences (steps) are shown in the range of 2.11 to 2.63 eV. The average between these steps is about $0.17 \text{ eV} \pm 0.02$.
- Similar steps were observed in the photovoltage response of the NPS device based on aluminum, which were related with the distribution sizes of the nanocrystalline silicon in the NPS layer (Yan et al., 2002).
- Two minima are seen at 1.47 eV and 1.85 eV. The first decrement of energy is due to the end of the contributions of bulk silicon and the start of the contributions of the NPS. The second decrement is due to the radiative recombination of charge carriers caused by the photoluminescence process (Wang et al., 1993; Zhang et al., 1993).

For NPS:n-Si devices, the photovoltage and photocurrent spectral response were very different than that of NPS devices fabricated from the p-Si substrate:

- The Cu:n-Si and Cu:NPS:n-Si devices showed similar behavior in terms of spectral response.
- Only the sharp peak at 1.2 eV is displayed in both spectra. It suggests that the energy band gap of NPS is similar to the energy band gap of silicon substrate or well, the contribution of the NPS to the photovoltaic effect is negligible. The absence of photocurrent from the NPS layer is attributed to the recombination of charge carriers due to the dangling bonds (Hwang et al., 2011).

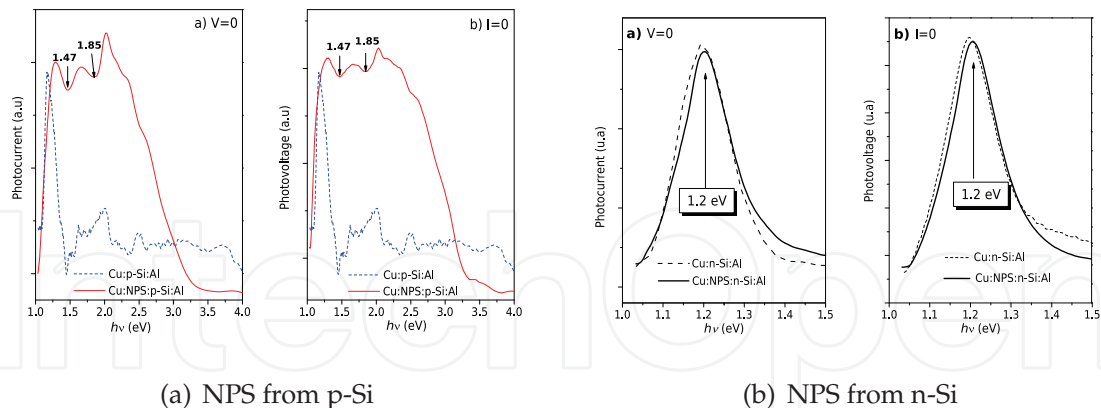


Fig. 15. Photocurrent and photovoltage of NPS devices from p-Si and n-Si (Arenas et al., 2008).

An energy diagram for NPS from p-Si (Fig. 16) is shown with the experimental data of E_g (≈ 1.88 eV) and the electronic affinity of NPS ($\chi \approx 3.6$ eV (Peng et al., 1996)). The data for crystalline silicon were also taken into account ($E_g=1.12$ eV): $E_F \approx 4.99$ eV for p-Si of 10 Ω -cm (Sze, 1990). The internal electrical field originated at the interface of the NPS:p-Si junction causes the opposite charge carriers to reach their respective metal contacts: electrons to Cu through NPS and holes to Al through p-Si. The photovoltage or photocurrent responses of the device were produced by the photogeneration of both electrons and holes in p-Si for photon energies greater than 1.12 eV and in NPS for energies greater than 1.8 eV.

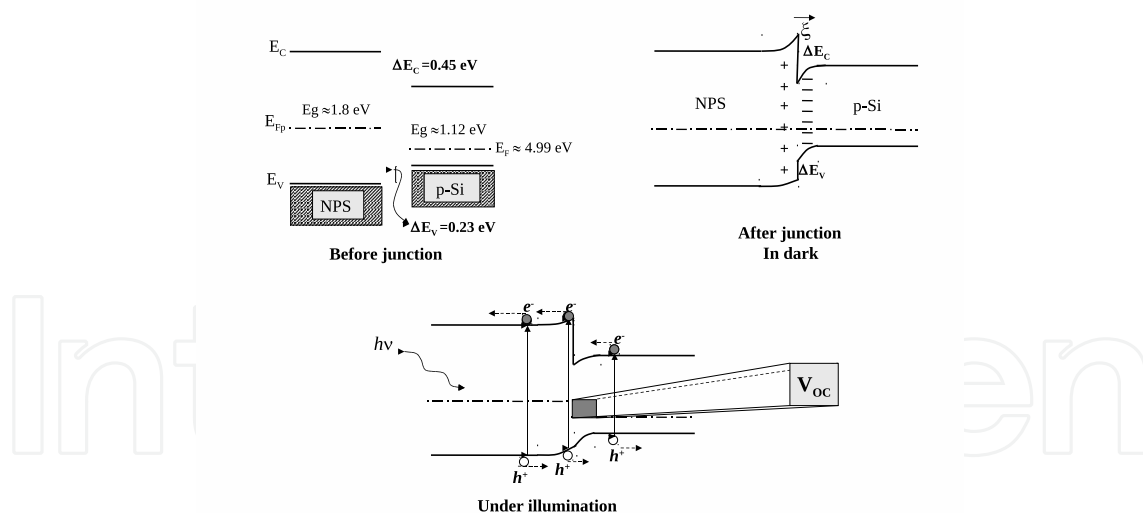


Fig. 16. Flat energy band diagrams of NPS devices based on p-Si before and after intimate contact and under illumination conditions.

5.3 Hybrid photovoltaic NPS:polypyrrole devices

A novel hybrid heterojunction based on NPS and polypyrrole (PPy) was proposed as a promising heterojunction for solar cell applications (Arenas et al., 2005; 2006;a; 2008). The conducting polymer improved the electroluminescent and photoluminescent

properties of NPS (Antipán & Kathirgamanathan, 2000; Bsiesy et al., 1995; Halliday et al., 1996; Parkhutik et al., 1994). The nanocrystallinity and the pore sizes are important parameters of the NPS layer because of their influence on the topography of the PPy:NPS devices and consequently the final performance of the PPy:NPS:n-Si devices (Arenas et al., 2006a):

- First, the photovoltaic response is present in PPy:n-Si devices without any NPS layer ($V_{oc}=135$ mV, $J_{sc}=8.58$ mA/cm²).
- The linear I - V curve trace under light is due to the high serial resistance (10⁴ ohms), and the efficiency conversion reached was 0.96%, as shown in Fig. 17a.
- The rough topography of the tip-like morphology of PPy:NPS devices leads to lower values of $V_{oc}=60$ mV and $J_{sc}=9.73 \times 10^{-3}$ mA/cm² compared to PPy:n-Si. The efficiency conversion was approximately $2 \times 10^{-4}\%$.
- A smooth and agglomerated morphology led to the following electrical parameters of the devices: $V_{oc}=95$ mV and $J_{sc}=0.13 \times 10^{-3}$ mA/cm².

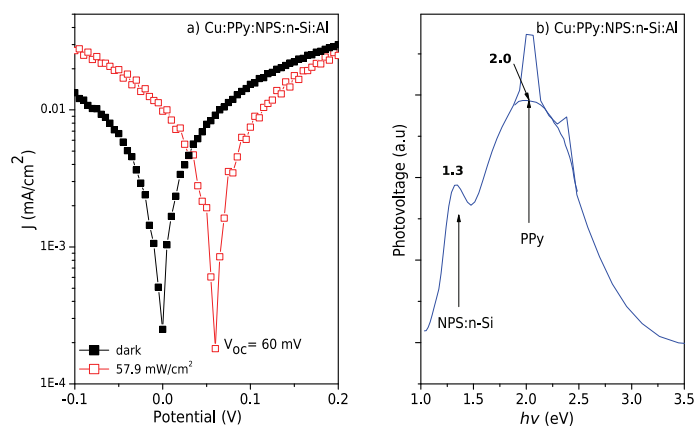


Fig. 17. a) J vs. V in dark and illumination conditions and b) photovoltage spectra of an NPS device based on polypyrrole.

The photovoltaic spectra displayed two peaks between 1 and 3 eV, as shown in Fig. 17b. The first acute peak is in the energies of 1 to 1.47 eV, and the second broad peak is at 1.47 to 3 eV, related to the contributions of the n-Si and PPy layers, respectively. The maximum peak at 1.9 eV corresponds to the energy band gap of PPy and is indicative of both components of the photogeneration of the charge carriers. The internal electrical field in the PPy:n-Si slightly aids the photogeneration of charge carriers.

6. Conclusion

This chapter focused on the preparation, characterization and systematic electrical evaluation of NPS based photovoltaic devices. The large surface area of NPS makes it a promising material for optoelectronic devices. The main structure of NPS is based on silicon crystals of nanometric size, which depend on which silicon type is used. Its experimental energy band gap of 1.8 eV leads to an absorption range in the visible spectra, which is an advantage if it is required as an active absorbing material in solar cells. The results shown in this chapter

demonstrate that NPS could represent a good alternative to develop solar cells based on hybrid heterojunctions. However, it is necessary to continue researching strategies to dope NPS to increase its electrical conductivity and therefore improve the conversion efficiency of hybrid devices.

7. Acknowledgments

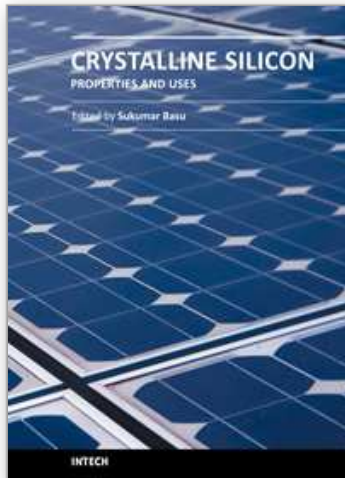
Antonio del Rio and Hailin Hu from CIE-UNAM by their advice, and IACOD-DGAPA (I1102611 project) for the financial support.

8. References

- Anderson, R.C., Muller, R.S. & Tobias, C.W. (1990). Investigations of porous silicon for vapor sensing, *Sensors and Actuators A: Physical* 23: 835-839.
- Antipán J. & Kathirgamanathan, P. (2000). White light electroluminescence from P Si devices capped with poly(thiophene)(s) as top contact, *Synthetic Metals* 110 (3): 233-240.
- Arenas, C., Hu, H., del Río, J. A., Salinas, O.H. & Sánchez, A. (2005). Porous silicon with conducting polymers for photovoltaic applications, *Proceedings of 20th European Photovoltaic Solar Energy Conference and Exhibition, Spain*, 220-222.
- Arenas, M. C., Hu, H., Del Río, J. A., Sánchez, A. & Nicho-Díaz, M. E. (2006). Electrical properties of porous silicon/polypyrrole heterojunctions, *Solar energy materials & solar cell* 90: 2413-2420.
- Arenas, M. C., Hu, H., del Río, J. A. & Nicho, M. E. (2006). Morphology Study of a hybrid structure base on porous silicon and polypyrrole, *Proceedings of Materials Research Society Symposium* 939: 0939-O03-22.
- Arenas, M.C., Hu, H., Del Río, J. A. & Salinas O. H. (2008). Photovoltage and J-V features of porous silicon, *Revista Mexicana de Física* 54(5): 391-396.
- Arenas, M. C., Hu, H., Nava, R., & del Río, J. A. (2010). Determination of the complex refractive index of porous silicon layers on crystalline silicon substrates, *International Journal of Modern Physics B* 24(24): 4835-4850.
- Bard, A. J. (1986). *Encyclopedia of Electrochemistry of the Elements*, Dekker, New York.
- Beckmann, K.H., (1965). Investigation of the chemical properties of stain films on silicon by means of infrared spectroscopy, *Surface Science* 3(4): 314-332.
- Bisi, O., Ossicini, S. & Pavesi, L. (2000). Porous silicon: a quantum sponge structure for silicon based optoelectronics, *Surface science reports* 38: 1-126.
- Brabec, C.J., Shaheen, S.E., Fromherz, T., Padinger, F., Hummelen, J.C., Dhanabalan, A., Jassen, R.A.J. & Sariciftci, N.S. (2001). Organic photovoltaic devices produced from conjugated polymer / methafullerene bulk heterojunctions, *Synthetic Metals* 121: 1517-1520.
- Bsiesy, A., Nicolau, Y.F., Ermolieft, A., Muller, F. & Gaspard, F. (1995). Electroluminescence from n^+ -type porous silicon contacted with layer-by-layer deposited polyaniline, *Thin Solid Films* 255:43-48.
- Bomchil, G., Herino, R., Barla, K. & Pfister J. C. (1983). Pore size distribution in porous silicon studied by adsorption isotherms, *Journal of Electrochemical Society* 130: 1611-1614.
- Canham, L.T. (1990). Silicon quantum wire array fabrication by electrochemical and chemical dissolution of wafers, *Applied Physics Letter* 57: 1046-1048.
- Carroll F. Powell, Joseph H. Oxley, Johj M. & Blocher Jr., (1966), *Vapor Deposition*, John Wiley & Sons.

- Conway, B.E., Bockris, J.O M., Yeager, E., Khan, S.U.M. & White, R.E. (1983). *Comprehensive Treatise of Electrochemistry* Plenum, New York.
- Dillon, A. C., Robinson, M. B., Han, M. Y. & George S. M. (1992). Diethylsilane Decomposition on silicon surfaces studied using Transmission FTIR spectroscopy, *Electrochemical Society* 139: 537-543.
- Eddowes, M. J. (1990). Anodic dissolution of p- and n-type silicon: Kinetic study of the chemical mechanism, *Journal of Electroanalytical Chemistry* 280: 297-311.
- Fauchet, P.M., Tsybescov, L., Duttagupta, S.P. & Hirshmann, K. D. (1997). Stable photoluminescence and electroluminescence from porous silicon, *Thin Solid Films* 297 (1-2): 254-260.
- Feng, Z. C. & Tsu, R. (1994). *Porous silicon*, World Scientific.
- Galun, E., Reuben, C., Matlis, S., Tenne, R. & Levy-Clement, C. (1995). Morphology of n-type macroporous silicon: doping density dependence, *Journal of Physical Chemistry* 99: 4132-4140.
- Gupta, P., Dillon, A.C., Bracker, A.S. & George S.M. (1991). FTIR studies of H_2O and D_2O decomposition on porous silicon surfaces, *Surface Science* 245: 360-372.
- Halliday, D. P., Holland, E. R., Eggleston, J. M., Adams, P.N., Cox, S.E. & Monkman, A.P. (1996). Electroluminescence from porous silicon using a conducting polyaniline contact, *Thin Solid Films* 276(1-2): 299-302.
- Heavens, O. S. (1965). *Optical properties of thin solid films*, Dover Publications.
- Holmes, P. J., (1962). *The Electrochemistry of Semiconductors*, Academic, London.
- Hwang, J.D., Hwang, S.B., Chou, C.H. & Chen, Y.H. (2011). Investigation of opto-electronic properties on gradient-porosity porous silicon layer, *Thin Solid Films* 519 (7): 2313-2316.
- Jung, K. G., Schultze, J. W., Thönissen, M. & Munder, H. (1995). Deposition of electrically conducting polybithiophene into porous silicon, *Thin Solid Films* 255: 317-320.
- Kordás, K., Pap. A. E., Beke, S. & Leppävuori, S., (2004). Optical properties of porous silicon (Part I) - Fabrication and investigation of single layers, *Optical Materials* 25(3): 251-255.
- Lehmann V., Föll, H. (1990). Formation Mechanism and properties of electrochemically etched trenches in n-type silicon, *Journal of Electrochemical Society* 137: 653-659.
- Lehmann, V. & Gösele, U. (1991). Porous silicon formation: a quantum wire effect, *Applied Physics Letters* 58: 856-858.
- Lugo, J. E., del Río, J. A. & Tagüe na-Martínez J. (1998) Surface contribution to the effective optical properties of porous silicon, *Solar Energy Materials and Solar Cells* 52(3-4): 239-249.
- Manificier, J.C., Gasiot, J. & Fillard, J.P. (1976). A simple method for the determination of the optical constants n, k, and the thickness of a weakly absorbing thin film, *Journal of Physics E: Scientific Instruments* 9(11): 1002.
- Moreno, J. D., Marcos, M.L. & Agulló-Rueda F. (1999). A galvanostatic study of the electrodeposition of polypyrrole into porous silicon, *Thin Solid Films* 348: 152-156.
- Murarka, S.P. (1983). *Silicides for VLSI Applications*, Academic Press, Inc.
- Nguyen, T.P., Le Rendu, P. & Cheah K. W. (2003). Optical properties of porous silicon/poly(p phenylene vinylene) devices, *Physica E* 17: 664-665.
- Parkhutik, V.P., Diaz Calleja, R., Matveeva, E.S. & Martinez-Duart, J.M. (1994). Luminescent structures of porous silicon capped by conductive polymers, *Synthetic Metals* 67: 111-114.

- Patterson, A.L. (1939). The Scherrer Formula for X-Ray Particle Size Determination, *Physical Review* 56 15: 978-982.
- Peng, C., Hirschman, K.D, Fauchet, P.M. (1996). Carrier transport in porous silicon light-emitting devices, *Journal of Applied Physics* 80(1): 295-300.
- Pierret, R.F. & Neudeck, G. W. (1989). *The PN Junction Diode*, Addison-Wesley Publishing Company.
- Rhoderick, E.H. & Williams, R.H. (1998). *Metal & Semiconductor contacts*, Clarendon Press Oxford.
- Sagnes, I., Halimaoui, A., Vincent, G. & Badoz, P.A., (1993). Optical absorption evidence of quantum size effect in porous silicon, *Applied Physics Letters* 62(10): 1155-1157.
- Salinas, O. H., López-Mata, C., Hu, H., Nicho, M. E. & Sánchez, A. (2006). Metal contact properties of poly(3-octylthiophene) thin films, *Solar Energy Material & Solar Cells* 90: 760-769.
- Schroder, D. K. (1998). *Semiconductor material and device characterization*, John Wiley & Sons.
- Searson, P. C., Macaulay, J. M. & Ross, F. M. (1992). Pore morphology and the mechanism of pore formation in n-type silicon, *Journal of Applied Physics* 72: 253-258.
- Smestad, G. & Kunst, M. (1992). Photovoltaic response in electrochemically prepared photoluminescent porous silicon, *Solar Energy Materials and Solar Cells* 26: 277-283.
- Smith, R. L. & Collins, S. D. (1992). Porous silicon formation mechanisms, *Journal of Applied Physics* 71: R1–R22.
- Swanepoel, R. (1983). Determination of the thickness and optical constants of amorphous silicon, *Journal of Physics E: Scientific Instruments* 6: 1214.
- Sze, S.M. (1990), *Physics of semiconductor devices*, John Wiley & Sons.
- Torres-Costa, V., Gago, R., Martín-Palma, R.J., Vinnichenko, M., Grötzschel, R., & Martínez-Duart, J.M. (2003). Development of interference filters based on multilayer porous silicon structures, *Materials Science and Engineering: C* 23(6-8): 1043-1046.
- Turner, D. R. (1958). Electropolishing silicon in hydrofluoric, *Journal of Electrochemical Society* 105: 402-408.
- Vijh, A.K. (1973). *Electrochemistry of Metals and Semiconductors*, Dekker, New York.
- Vitanov, P., Kamenova, M., Tyutyundzhiev, N., Delibasheva, M., Goranova, E. & Peneva M. (1997). High-efficiency solar cell using a thin porous silicon layer, *Thin solid Films* 297: 299-303.
- Wang, X., Huang, D., Ye, L., Yang, M., Hao, P., Fu, H., Hou, X. & Xie, X. (1993). Pinning of photoluminescence peak positions for light-emitting porous silicon: An evidence of quantum size effect, *Physical Review Letters* 71(8): 1265-1267.
- Wolfgang R. (1991). *Electroless Nickel Plating*, ASM International.
- Yan, F., Bao, X.-M. & Gao, T. (2002). Photovoltage spectra of silicon/porous silicon heterojunction, *Solid State Communications* 91(5): 341-343.
- Yu, Z. & Wie, C.R. (1992). Fabrication of MSM photoconductor on porous Si using micromachined silicon mask, *Electronics Letter* 28: 911-913.
- Zhang, S.-L., Ho, K.-s., Hou, Y., Qian, B., Diao, P. & Cai, S. (1993). Steplike behavior of photoluminescence peak energy and formation of p-type porous silicon, *Applied Physics Letters* 62(6): 642-644.



Crystalline Silicon - Properties and Uses

Edited by Prof. Sukumar Basu

ISBN 978-953-307-587-7

Hard cover, 344 pages

Publisher InTech

Published online 27, July, 2011

Published in print edition July, 2011

The exciting world of crystalline silicon is the source of the spectacular advancement of discrete electronic devices and solar cells. The exploitation of ever changing properties of crystalline silicon with dimensional transformation may indicate more innovative silicon based technologies in near future. For example, the discovery of nanocrystalline silicon has largely overcome the obstacles of using silicon as optoelectronic material. The further research and development is necessary to find out the treasures hidden within this material. The book presents different forms of silicon material, their preparation and properties. The modern techniques to study the surface and interface defect states, dislocations, and so on, in different crystalline forms have been highlighted in this book. This book presents basic and applied aspects of different crystalline forms of silicon in wide range of information from materials to devices.

How to reference

In order to correctly reference this scholarly work, feel free to copy and paste the following:

Ma. Concepción Arenas-Arrocena, Marina Vega-Gonzalez, Omar Martinez and Oscar H. Salinas-Aviles (2011). Nanocrystalline Porous Silicon: Structural, Optical, Electrical and Photovoltaic Properties, Crystalline Silicon - Properties and Uses, Prof. Sukumar Basu (Ed.), ISBN: 978-953-307-587-7, InTech, Available from: <http://www.intechopen.com/books/crystalline-silicon-properties-and-uses/nanocrystalline-porous-silicon-structural-optical-electrical-and-photovoltaic-properties>

INTECH
open science | open minds

InTech Europe

University Campus STeP Ri
Slavka Krautzeka 83/A
51000 Rijeka, Croatia
Phone: +385 (51) 770 447
Fax: +385 (51) 686 166
www.intechopen.com

InTech China

Unit 405, Office Block, Hotel Equatorial Shanghai
No.65, Yan An Road (West), Shanghai, 200040, China
中国上海市延安西路65号上海国际贵都大饭店办公楼405单元
Phone: +86-21-62489820
Fax: +86-21-62489821

© 2011 The Author(s). Licensee IntechOpen. This chapter is distributed under the terms of the [Creative Commons Attribution-NonCommercial-ShareAlike-3.0 License](#), which permits use, distribution and reproduction for non-commercial purposes, provided the original is properly cited and derivative works building on this content are distributed under the same license.

IntechOpen

IntechOpen